NASA Technical Memorandum 105697
AIAA–92–3789

Experimental Performance of Three Design Factors for Ventral Nozzles for SSTOVL Aircraft

Barbara S. Esker and Gail P. Perusek
Lewis Research Center
Cleveland, Ohio

Prepared for the
28th Joint Propulsion Conference and Exhibit
cosponsored by the AIAA, SAE, ASME, and ASEE
Nashville, Tennessee, July 6–8, 1992

NASA

Flow was confined to an annular path that was 69 percent of the baseline tailpipe flow area. This configuration simulated a separate flow condition in which the ventral nozzle is supplied with fan flow only.

The shortened tailpipe configuration shown in Fig. 5 varied from the baseline with the addition of a blocker mounted in the tailpipe. This addition effectively moved the location of the aft blind flange to 2 in. downstream of the ventral opening. This blocker was constructed from a 3/4-in. plywood disk braced in position with wooden struts. The effect was to reduce the volume of the recirculation region in the aft end of the tailpipe by 93 percent. This configuration simulated a tailpipe blocker mechanism placed immediately downstream of the ventral duct as opposed to a closed cruise nozzle.

The short ventral duct configuration is shown in Fig. 6. This configuration varied from the baseline with the removal of a rectangular spool to reduce the length of the ventral duct by 33 percent. The configuration simulated ventral duct lengths more closely designed to fit in an aircraft fuselage.

Test Facility

The Powered Lift Facility (PLF) (shown in Fig. 2) consists of a high-pressure air supply and a thrust balance system. The thrust system can simultaneously measure thrust in the vertical, axial, and lateral directions and can measure moments about all three axes. The ventral nozzle model was supplied with cold (approx. 70 °F), high-pressure air from the Lewis central air supply system at pressures up to 90 psig and 100 lb/sec at the model. See Appendix A for a more detailed description of the PLF.

Instrumentation and Data Processing

The location and number of total pressure instrumentation for the baseline ventral configuration are shown in Fig. 3. This same instrumentation was maintained for all configurations, except for those instrumented pieces that were removed for a particular test. The total pressure at the tailpipe reference location (station 5) was measured by using 20 total pressure tubes located on centers of equal area. Similarly, there were 24 total pressure tubes located on centers of equal area at the ventral nozzle inlet (station 6). A five-tip total pressure rake was used to obtain a pitot pressure survey at the ventral nozzle exit plane (station 6B). Static pressure measurements were made in the tailpipe and ventral duct. The total temperature was measured just upstream of the transition section and was assumed to be constant throughout the model.

All steady-state pressure data were scanned by an electronic data acquisition system at a rate of one scan per second. Dynamic pressure data were not obtained. Data were batch processed on the Lewis mainframe computer system.

Experimental Procedure

Performance Tests

Performance testing consisted of measuring the thrust and flow characteristics of the ventral nozzle systems over a range of several tailpipe-to-ambient-pressure ratios (PR_5) up to 5.0.

Flow Visualization

Flow visualization studies were performed on the annular flow duct, shortened tailpipe, and shortened ventral duct configurations. These studies used white oil paint mixed with a light oil to provide a smooth mixture that was able to hold its shape on the underside of walls and vertical surfaces. The dabs of paint were applied to internal surfaces of interest, such as the duct walls and centerbody. For the plane-of-symmetry flow visualization, a rectangular pattern of paint dabs was used on a flat plate which mounted vertically in the tailpipe along the centerline of the duct. The system pressure was increased quickly from ambient to approximately a tailpipe-to-ambient pressure ratio (PR_5) of 3.0 (high enough to choke the ventral nozzle), was held for about 30 sec, and then brought back to ambient. The flow caused the paint to travel along streamlines, providing a clear picture of the flow pattern. Photographs were then taken of these paint-streak patterns.

Exit Plane Survey

Pitot pressure surveys of the ventral nozzle exit plane were performed by using the five-port total pressure rake at a tailpipe-to-ambient-pressure ratio of 3.0. An actuator was used to traverse the rake axially (parallel to the tailpipe axis) across the ventral nozzle exit. After each axial traverse, the assembly (probe and actuator) was moved laterally across the exit plane in 3-in. increments. Surveys were taken across the entire nozzle exit plane on the shortened ventral duct configuration and across half of the nozzle exit plane on the annular flow duct configuration.

CFD Analysis of Shortened Ventral Duct

Computational Grid

A computational fluid dynamics analysis was done on the short ventral duct configuration. The grid used for this analysis is shown in Fig. 7. This grid comprised two blocks: the cylindrical tailpipe and the rectangular ventral duct and nozzle. It contained a total of 525 402 nodal points (tailpipe: 101 by 51 by 51; ventral duct and nozzle: 51 by 51 by 101). Because of a plane of symmetry in the experimental hardware, only one-half of the configuration was modeled for the computational analysis. The grid was a variation of the original ventral nozzle grid which is discussed in Refs. 1 to 4. The modification consisted of compressing the ventral duct grid in the vertical direction by using INGRID3D.[6]

PARC3D Code

The analysis was done using the full Navier-Stokes code PARC3D.[5] PARC3D solves the Reynolds-averaged Navier-Stokes equations and employs the Beam-Warming approximate factorization scheme. Turbulence was simulated by using the Baldwin-Lomax turbulence model[7] for wall-bounded flows. The blocked version of PARC3D was run on the Lewis Cray Y-MP computer. This blocked version of the code allowed the computational domain to be divided into several simple blocks. Each block was solved separately, and a trilinear interpolation scheme transferred data across adjacent block boundaries.

Boundary Conditions

The boundary condition used for the computational analysis of the short ventral duct configuration included a fictitious diverging section at the exit of the ventral nozzle (not shown in Fig. 7). The diverging section allowed the flow to expand to supersonic speeds and allowed the conditions at the fictitious exit plane to be extrapolated. This technique was used to avoid placing a set boundary condition at the actual exit plane of the nozzle and has been used previously with good results.[1-4]

Another boundary condition used for this analysis was a pole boundary condition located at the center of the tailpipe grid. Because the tailpipe was modelled using an O-grid, the grid lines become coincident at the center and problems calculating metrics occur. The pole boundary condition was created so that the flow properties on this boundary were calculated by averaging the values along the adjacent grid lines.

Results and Discussion

Tailpipe Mach Number

Figure 8 shows the Mach number in the tailpipe for the four ventral nozzle configurations. The baseline, shortened tailpipe, and short ventral duct have a tailpipe Mach number of approximately 0.3 at tailpipe-to-ambient-pressure ratios PR_5 above 2.5. The annular flow duct configuration resulted in a tailpipe Mach number of approximately 0.42 for a PR_5 greater than 2.5. The 0.42 Mach number resulted from the centerbody that reduced the tailpipe flow area. Because of the significant pressure loss between the tailpipe and ventral duct for all configurations, the ventral nozzle did not choke until a PR_5 of 2.5.

Total Pressure Loss

The pressure losses through three ventral nozzle systems are shown in Fig. 9. The pressure loss was defined as

$$\text{Total pressure loss} = \frac{\text{Tailpipe reference pressure} - \text{Ventral nozzle inlet pressure}}{\text{Tailpipe reference pressure}}$$

At a PR_5 of 3.0, the pressure losses for the three configurations were 5.6 percent (baseline), approximately 6.1 percent (shortened tailpipe), and approximately 5.0 percent (short ventral duct). The PARC3D result for pressure loss through the short ventral duct configuration was 4.4 percent. The total pressure loss for the annular flow duct configuration was not calculated because the total pressure rake at the ventral nozzle inlet broke as a result of unexpected, severe flow angles. The rake was repaired for the testing of the later configurations.

System Discharge Coefficient

Figure 10 gives the discharge coefficients for the four ventral nozzle systems over a range of tailpipe-to-ambient pressure ratios. For the nozzle system, the discharge coefficient (C_D) was defined as

$$C_D = \frac{\text{Actual flow rate}}{\text{Ideal flow rate calculated using measured tailpipe pressure}}$$

For all configurations, the total temperature of the airflow was approximately 70 °F. The baseline discharge coefficient was 0.901 at a tailpipe pressure ratio of 3.0. The annular flow duct configuration showed a significant decrease in flow performance with a system discharge coefficient of 0.845, 5 percent lower than that of the baseline. Both the shortened tailpipe and the short ventral duct configurations had discharge coefficients very similar to that of the baseline. The shortened tailpipe configuration was slightly lower ($C_D = 0.898$) whereas the short ventral duct configuration was slightly higher ($C_D = 0.905$) at a PR_5 of 3.0. The PARC3D discharge coefficient for the short ventral duct configuration was 0.903 and agreed very well with the experimental result.

Thrust

For the three ventral configurations studied, the corrected vertical thrust as a fraction of the corrected vertical thrust from the baseline is given in Fig. 11. The annular flow duct configuration produced the least vertical thrust, 91 percent of the vertical thrust of the baseline at a PR_5 of 3.0. As with the discharge coefficient, the results were similar for the shortened tailpipe and the short ventral duct configurations. The shortened tailpipe configuration produced 99 percent and the short ventral duct configuration produced 100 percent of the vertical thrust of the baseline. The PARC3D result was 99.3 percent of the baseline, slightly lower than the experimental result for the short ventral duct configuration.

Figure 12 gives the ratio of the corrected thrust to the corrected flow for each configuration relative to the baseline configuration. This relationship is expressed as

$$\frac{\dfrac{\text{Corrected thrust}}{\text{Corrected flow}}}{\left(\dfrac{\text{Corrected thrust}}{\text{Corrected flow}}\right)_{\text{Baseline}}}$$

The annular flow duct configuration produced less thrust for a given flow, approximately 97 percent of the baseline at a PR_5 of 3.0. Also, at a PR_5 of 3.0, the shortened tailpipe and the short ventral duct configurations produced the same thrust for a given flow as that produced by the baseline configuration.

The results of the baseline configuration reported in Refs. 1 to 4 indicated that the ventral jet overturned (turned more than 90 deg), and the system produced an axial force component. Similar results were obtained with the three variations to the ventral system. The axial force as a percent of vertical force for each of the configurations is given as Fig. 13. The baseline produced 7 percent axial thrust at a PR_5 of 3.0. The annular flow duct configuration produced 12 percent axial thrust. The shortened tailpipe and short ventral duct configurations produced less axial thrust than the baseline, 5.5 and 5 percent, respectively. In comparison to the experimental result for the short ventral duct configuration, the PARC3D result indicated a slightly higher axial thrust, 6 percent of the vertical thrust.

Flow Visualization

Flow visualization results on the front and side walls of the ventral duct in the annular flow duct configuration are shown in Figs. 14(a) and (b), respectively. These figures reveal the very complicated vortices in the ventral duct. The flow visualization on the front wall indicated that the flow along this wall was strongly inboard and upward into the ventral duct. Figure 14(b) shows the significant flow angle as the tailpipe flow overturned entering the ventral duct. Also, this figure shows reverse flow, that is, flow that bypassed the ventral duct initially, turned around in the aft portion of the tailpipe, and then exited the ventral duct. Apparent in both Figs. 14(a) and (b) are two vortices located on the ventral side of the centerbody. These vortices are counterrotating and develop from both oncoming tailpipe flow and reverse flow.

Figures 15(a) and (b) show the flow visualization for the front and side walls, respectively, of the ventral duct for the shortened tailpipe configuration. The flow visualization on the front wall shows that the flow is primarily inboard. Two small counterrotating vortices are apparent. These are located close to the plane of symmetry near the opening from the tailpipe. Figure 15(b) shows the flow overturning in the ventral duct.

Two types of flow visualization (on the internal walls and on the plane of symmetry) were done on the short ventral duct configuration in order to provide a more complete comparison with the PARC3D results. The streamline pattern from the plane-of-symmetry flow visualization is seen in Fig. 16(a). The corresponding particle trace pattern, computed with the PARC3D code, is seen in Fig. 16(b). The experimental and the computational results agree very well. Both results show the flow turned smoothly into the ventral duct, separating from the front wall. Some tailpipe flow impacted the tailpipe wall just downstream of the ventral opening and reversed direction to exit through the ventral duct. Airflow from the side of the tailpipe opposite the ventral duct was diagonal past the ventral opening and into the recirculation region. This flow then returned forward along the opposite side of the tailpipe. Both results show a vortex located in the

ventral side of the tailpipe downstream of the ventral opening. This vortex formed from tailpipe flow entering the recirculation region and from the forward flow.

Flow visualization on the walls of the ventral duct for the short ventral duct configuration is shown in Fig. 17. The experimental and PARC3D results for the front ventral duct wall are given in Figs. 17(a) and (b). Both results show that the flow along the front wall is very strongly inboard and diagonally upward into the ventral duct. This flow was then pulled into a vortex located near the opening from the tailpipe. Flow visualization on the side wall of the ventral duct is shown in Fig. 17(c), and the corresponding particle trace, computed by PARC3D, is shown in Fig. 17(d). The experimental and anayltical results agree well. Both images show the overturning of the airflow in the ventral duct and are similar to the patterns on the ventral duct side walls of the previously discussed configurations.

Exit Plane Survey

Figure 18 gives the experimental contour plot of pitot pressures at the exit plane of the ventral nozzle for the annular flow duct configuration. This figure shows only one-half of the actual exit area because the five-tip total pressure rake failed (as a result of severe flow angles) while obtaining the second half of the data. However, a mirror-image flow pattern can be assumed to exist on the other side of the plane of symmetry. The contours represent the pitot pressure as a fraction of the tailpipe reference pressure. For the annular flow duct configuration, the pressure distribution at the exit plane included a large low-pressure region located along the forward wall of the ventral duct and nozzle. This low-pressure region extended over nearly 40 percent of the nozzle exit area. The minimum pressure in this region was approximately 80 percent of the tailpipe reference pressure. The maximum pressure at the exit plane was approximately 97.5 percent of the reference pressure.

For the short ventral duct configuration, the experimental contour plot of pitot pressures is shown in Fig. 19(a). These results showed a low-pressure region which was smaller (extending over approx. 25 percent of the nozzle exit area) but contained a lower minimum pressure (75 percent of the reference pressure) than the low-pressure region in the annular flow duct configuration. However, the maximum pressure at the ventral nozzle exit plane in this configuration was 100 percent of the tailpipe reference pressure. The lower minimum pressure and the higher maximum pressure resulted in steeper gradients at the exit plane for the short ventral duct configuration.

The total-pressure contour plot at the exit plane of the ventral nozzle, as computed by the PARC3D, is given in Fig. 19(b). This result is similar to the experimental result in Fig. 19(a) except for the effect of the shock loss in the experiment. Both results show a large low-pressure region and the steep gradients surrounding it. Also, the results both show regions of slightly lower pressure near the outer edge and along the back wall of the nozzle.

Conclusions

Three design variations of a generic ventral nozzle model were tested on the Powered Lift Facility at NASA Lewis Research Center. These variations included an annular flow path into the ventral duct, a tailpipe blocked immediately downstream of the ventral duct, and a shortened ventral duct length. In addition, a CFD analysis was done on the shortened ventral duct configuration. Results included thrust and flow performance, flow visualization, and pressure distributions at the exit of the ventral nozzle.

The results of this work could be used in the analysis of a ventral system for an aircraft. The goals of such a system would include (1) minimize internal pressure losses, (2) maximize vertical thrust produced, and (3) possibly minimize the axial component of the net ventral thrust (i.e., to minimize the need to control this force in an actual aircraft).

With these goals in mind, a summary of the performance of the ventral systems as compared to the performance of the baseline configuration follows:

1. The short ventral duct configuration had the best performance of the three configurations. In comparison to the baseline, this configuration showed less internal pressure loss and a slightly higher discharge coefficient. Also, this configuration produced the same vertical thrust and a smaller axial thrust component. These results tend to indicate that the ventral duct can be shortened without adversely affecting the flow and thrust performance.

2. The shortened tailpipe configuration (with the tailpipe blocked immediately downstream of the ventral duct) showed more internal total-pressure loss and slightly less system discharge coefficient. This configuration produced slightly less vertical thrust than the baseline and less axial thrust component. This elimination of the recirculation region had a slight adverse affect on the performance of the ventral system.

3. The annular flow duct configuration had a significantly lower discharge coefficient than the baseline configuration. The thrust produced by this configuration had less vertical component and more horizontal component than the thrust produced by the baseline

configuration. These results indicate that the attempt to draw flow from an annulus and direct it into the ventral duct resulted in a configuration with substantially worse performance than one in which the full-duct, cross-section of tailpipe flow is redirected.

Appendix A—Powered Lift Facility

This appendix gives a brief description of the more important features of the Lewis Research Center Powered Lift Facility (PLF).

The Powered Lift Facility (Fig. 2) can simultaneously measure thrust force levels in the vertical, axial, and lateral directions and can measure moments about all three axes (i.e., roll, pitch, and yaw). Not shown in Fig. 2 is the 65-ft-radius, acoustically treated, geodesic dome barrier to keep test noise from affecting neighboring communities. Also not shown in Fig. 2 is a work platform mounted underneath the frame to facilitate model buildup and configuration changes and to maintain a safe work enviroment. This work platform does not contact any of the thrust frame components and has removable grating in the center to allow nozzles to be directed downward.

Multi-Axis Thrust Measuring System

The PLF thrust frame is triangular shaped, 30 ft on a side, and stands 15 ft off the ground. The force balance is capable of measuring up to 60 000 lb vertically, 25 000 lb axially, and 10 000 lb laterally. Experimental hardware can weigh up to 40 000 lb. Only steady-state loads can be measured and aerodynamic effects (i.e., recirculation effects) of exhaust are negligible. The grating in the center of the work platform is removed when nozzles are directed downward, allowing a high degree of flexibility for nozzle exhaust direction and placement. Nozzles may exhaust axially (parallel with the ground plane out the dome exhaust door), downward, or back toward the facility inlet piping. In the last case, flow deflectors are required. Directing nozzles upward is not desirable because of the proximity of the dome wall.

Air Supply System

The PLF air supply system is seen in Fig. 20. Facility capabilities allow experimental hardware inlet pressures up to 90 psig and flow rates up to 150 lb/sec. The air supplied by the Lewis central air equipment building is at ambient temperatures and enters the facility through an isolation valve that is operated with a permissive from the central air system control. Flow rate is controlled with a 14-in. butterfly valve in the supply line downstream of the isolation valve. The flow rate is measured with a 9.125-in.-diameter ASME flow measuring nozzle located upstream of the butterfly valve. Flow measurement with the nozzle is accurate to within ± 0.5 percent including both scatter and systematic errors.

Instrumentation and Data Processing

Steady-state pressures are measured by an electronically scanned pressure (ESP) system with 372 available data channels. Up to 200 analog signals, which include strain gage transducers and thermocouple data, are available. The steady-state data acquisition system has a sampling rate of one scan (all analog and pressure channels) per second. Data are stored on a disk locally, then batch processed off-line using the Lewis mainframe computer system.

References

1. McArdle, J.G., and Smith, C.F., "Experimental and Analytical Study of Close-Coupled Ventral Nozzle for ASTOVL Aircraft," NASA TM-103170, Aug. 1990.

2. McArdle, J.G., and Smith, C.F., "Flow Studies in Close-Coupled Ventral Nozzles for STOVL Aircraft," SAE 901033, Apr. 1990.

3. Smith, C.F., and McArdle, J.G., "Analysis of Internal Flow in a Ventral Nozzle for STOVL Aircraft," AIAA Paper 90-1899, July 1990.

4. Smith, C.F., and McArdle, J.G., "Analysis of Internal Flow in a Ventral Nozzle," Journal of Propulsion and Power, Vol. 8, No. 2, Mar./Apr. 1992, pp. 530-536.

5. Cooper, G., and Sirbaugh, J., "The PARC Distinction: A Practical Flow Simulator," AIAA Paper 90-2002, July 1990.

6. Soni, B.K., "Two- and Three-Dimensional Grid Generation for Internal Flow Application of Computational Fluid Dynamics," AIAA Paper 85-1526, July 1985.

7. Baldwin, B.S., and Lomax, H., "Thin-Layer Approximation and Algebraic Turbulence Model for Separated Turbulent Flows," AIAA Paper 78-257, Jan. 1978.

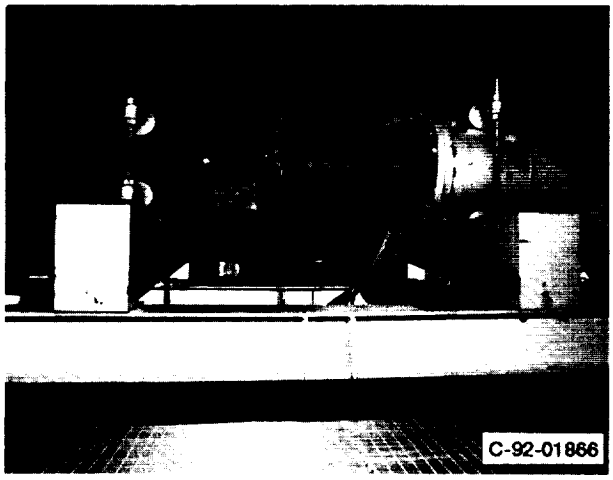

Figure 1.—Ventral nozzle baseline configuration mounted on the Powered Lift Facility.

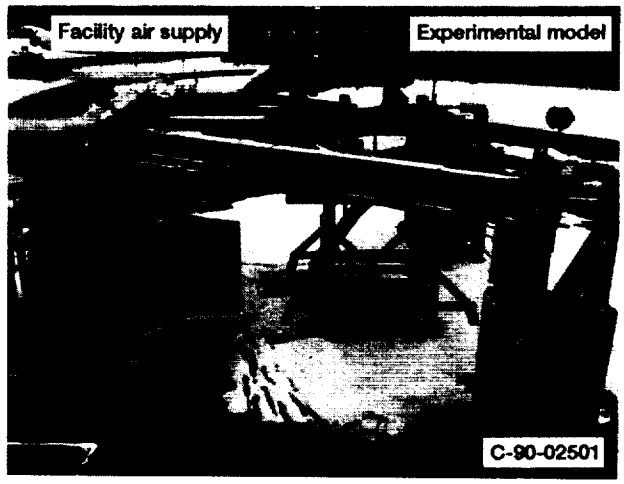

Figure 2.—Powered Lift Facility at NASA Lewis Research Center.

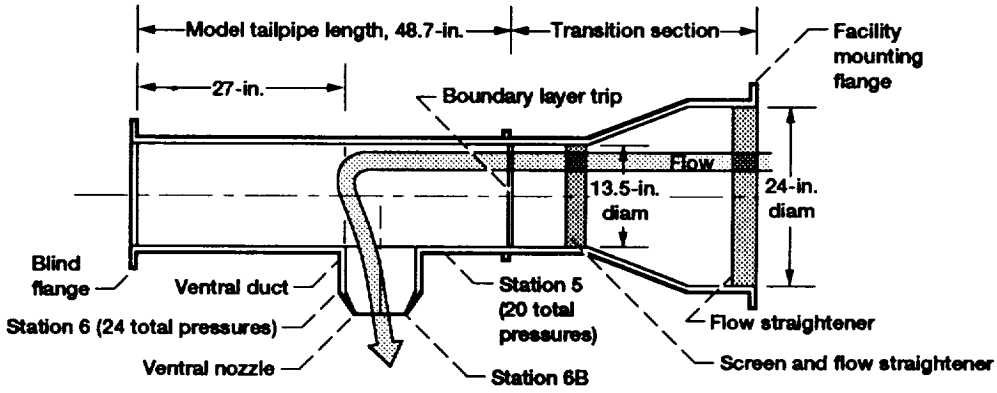

Figure 3.—Baseline ventral nozzle configuration.

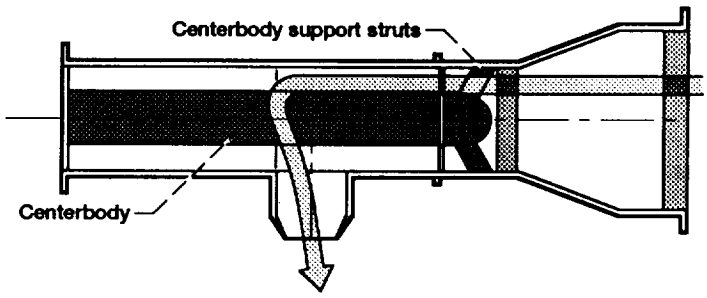

Figure 4.—Annular flow duct configuration.

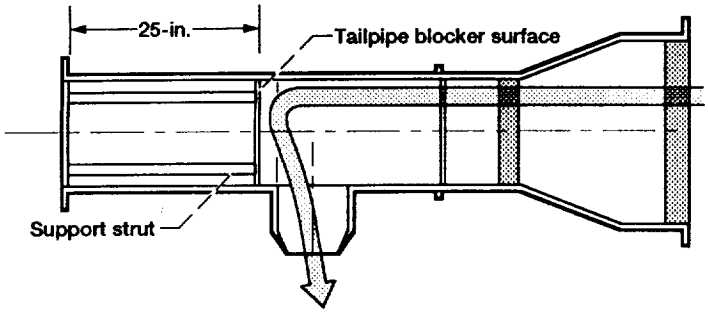

Figure 5.—Shortened tailpipe configuration.

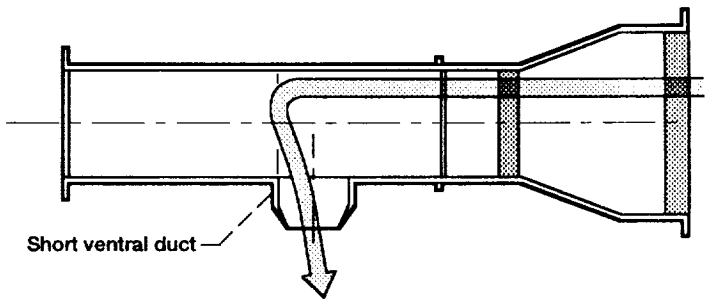

Figure 6.—Short ventral duct configuration.

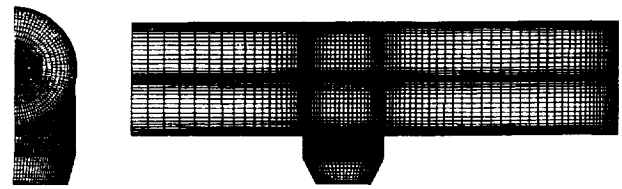

Figure 7.—Computational grid. Short ventral duct configuration.

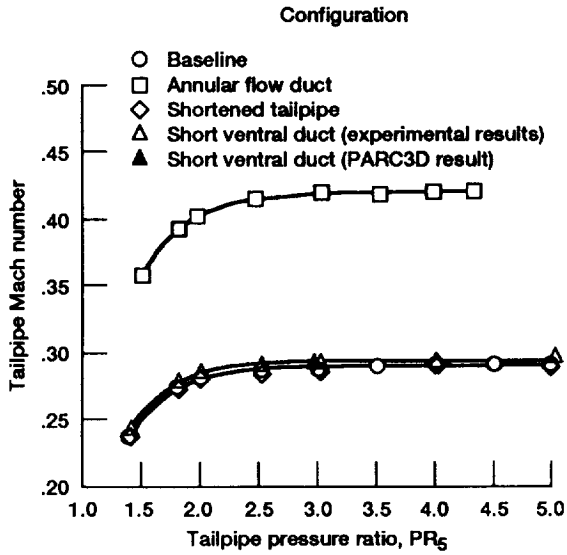

Figure 8.—Tåilpipe Mach number.

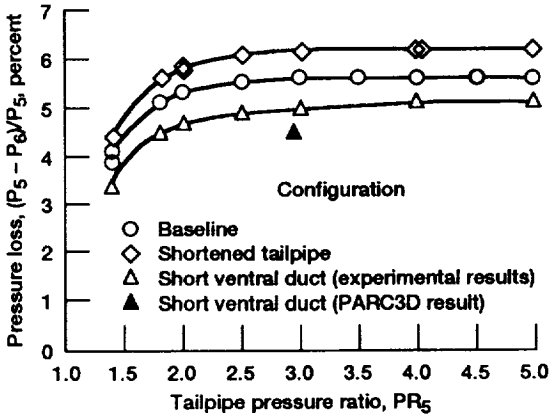

Figure 9.—System total pressure loss.

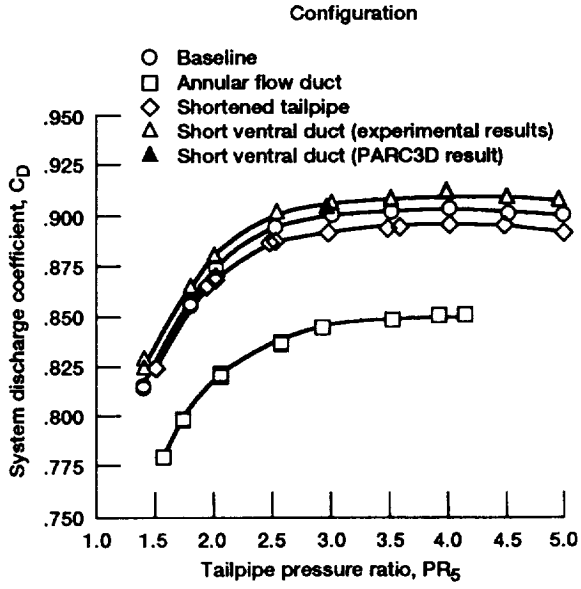

Figure 10.—Discharge coefficient.

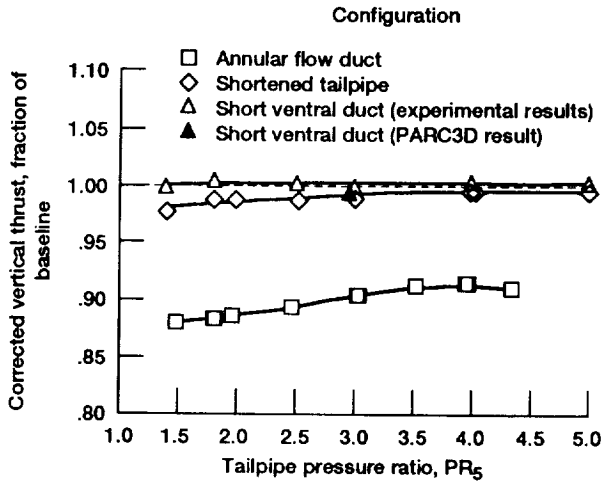

Figure 11.—Corrected vertical thrust relative to corrected vertical thrust of baseline.

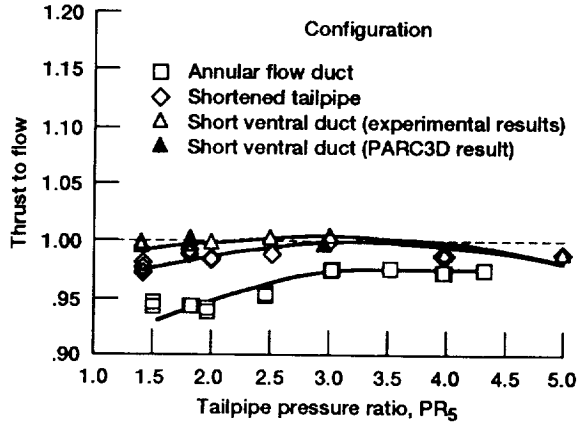

Figure 12.—Corrected thrust to corrected flow relative to the baseline configuration.

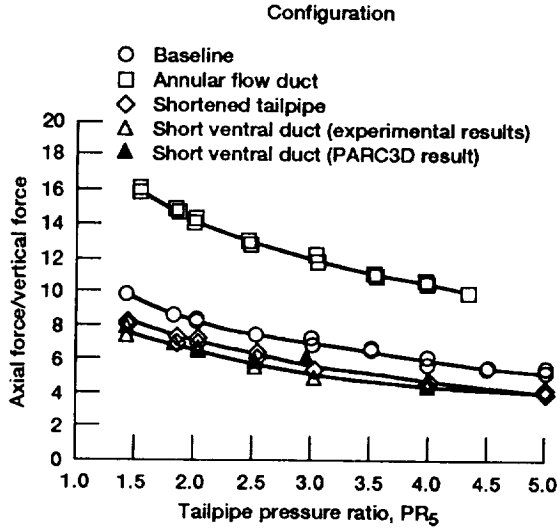

Figure 13.—Axial force as a percentage of vertical force.

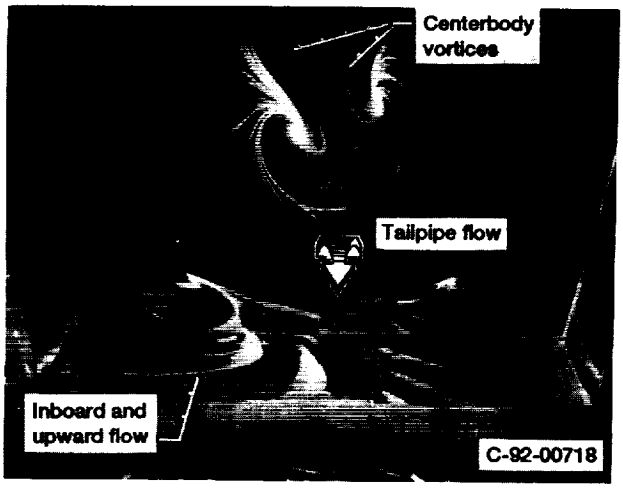

(a) Front wall.

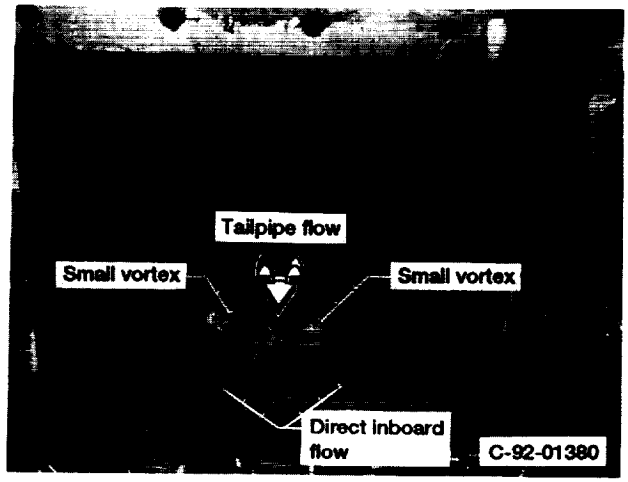

(a) Front wall.

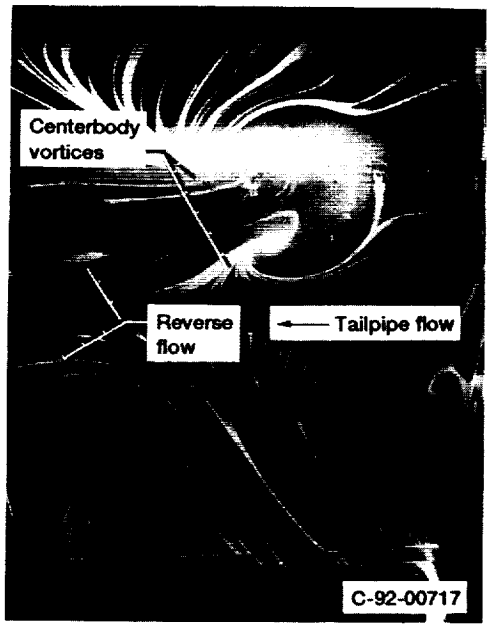

(b) Side wall.

Figure 14.—Annular flow duct configuration. Flow visualization of the ventral duct.

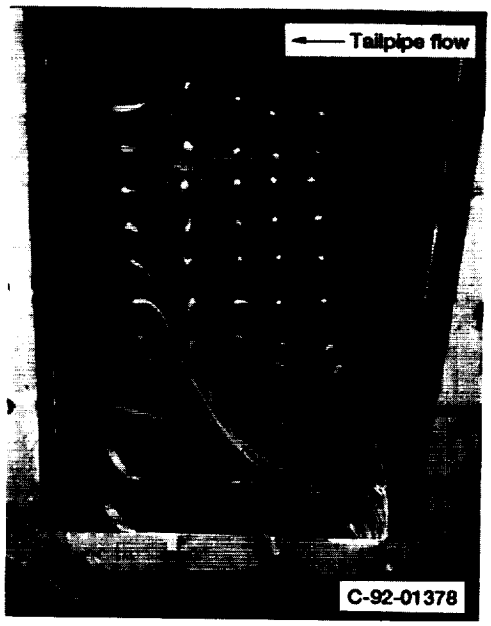

(b) Side wall.

Figure 15.—Shortened tailpipe configuration. Flow visualizations in the ventral duct.

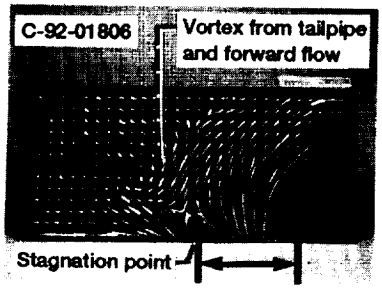

(a) Experimental result.

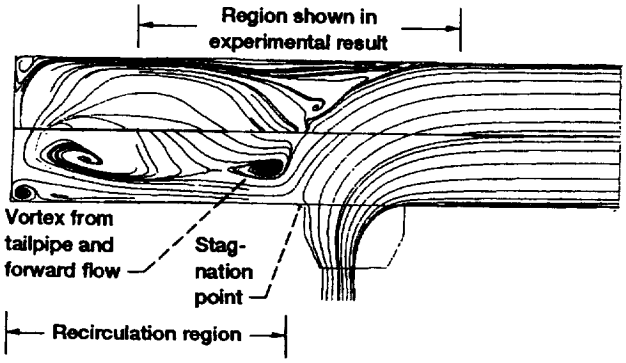

(b) PARC3D result.

Figure 16.—Flow visualization on the plane of symmetry for the short ventral duct configuration.

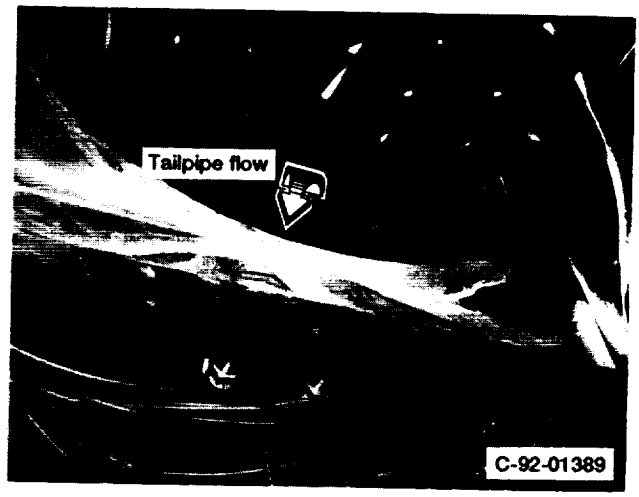

(a) Experimental results on front wall.

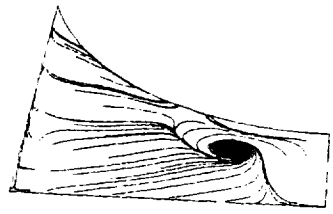

(b) PARC3D results on front wall.

Figure 17.—Short ventral duct configuration. Flow visualization of ventral duct.

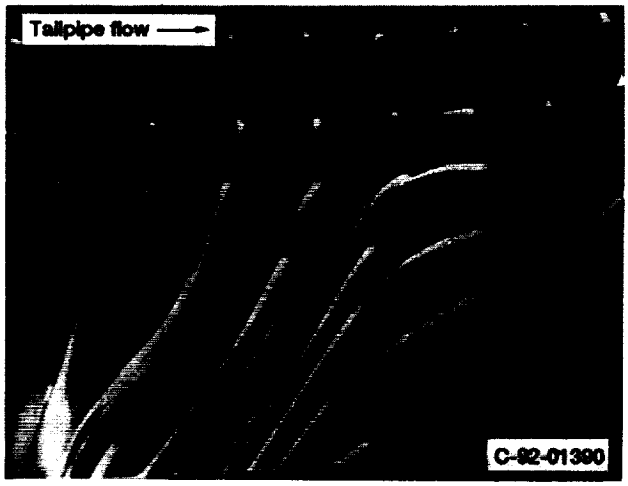

(c) Experimental results on side wall.

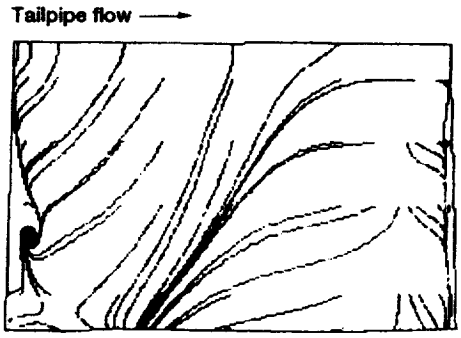

(d) PARC3D results on side wall.

Figure 17.—Concluded.

	Contour levels, P/P_{ref}		Contour levels, P/P_{ref}
A	0.750	G	0.900
B	.775	H	.925
C	.800	I	.950
D	.825	J	.975
E	.850	K	1.000
F	.875		

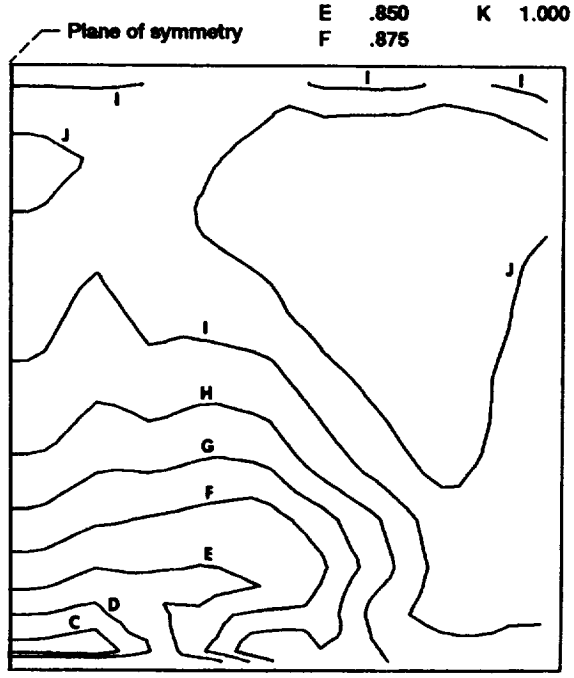

Figure 18.—Annular flow duct configuration. Contour plot of experimental pitot pressures at the ventral nozzle exit plane. Looking upstream into flow.

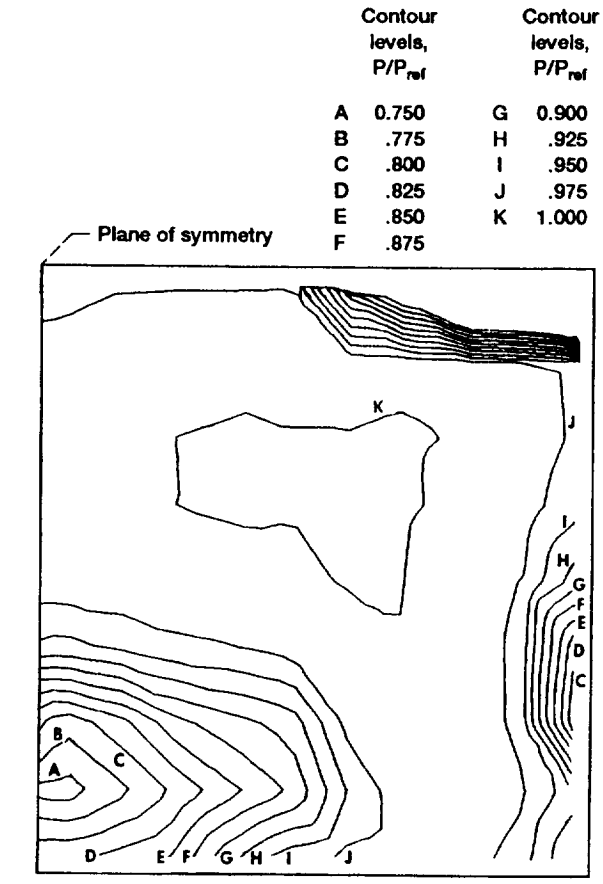

(a) Pitot pressures, experimental result.

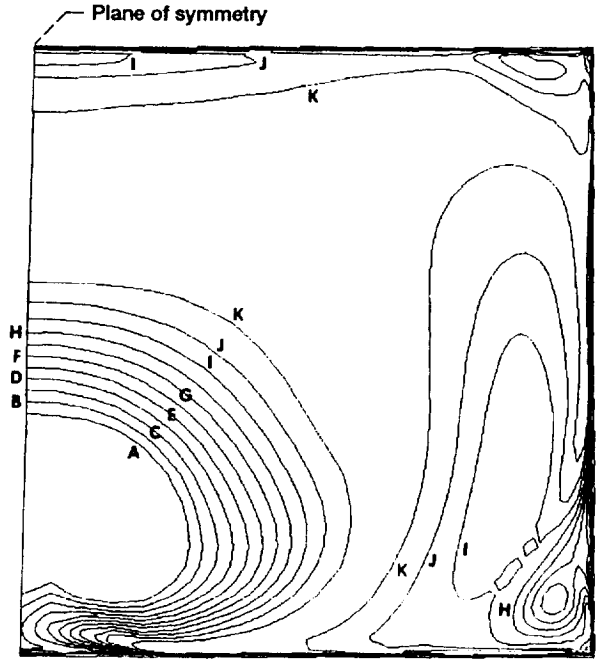

(b) Total pressures, PARC3D result.

Figure 19.—Short ventral duct configuration. Contour plots of ventral nozzle exit plane. Looking upstream into flow.

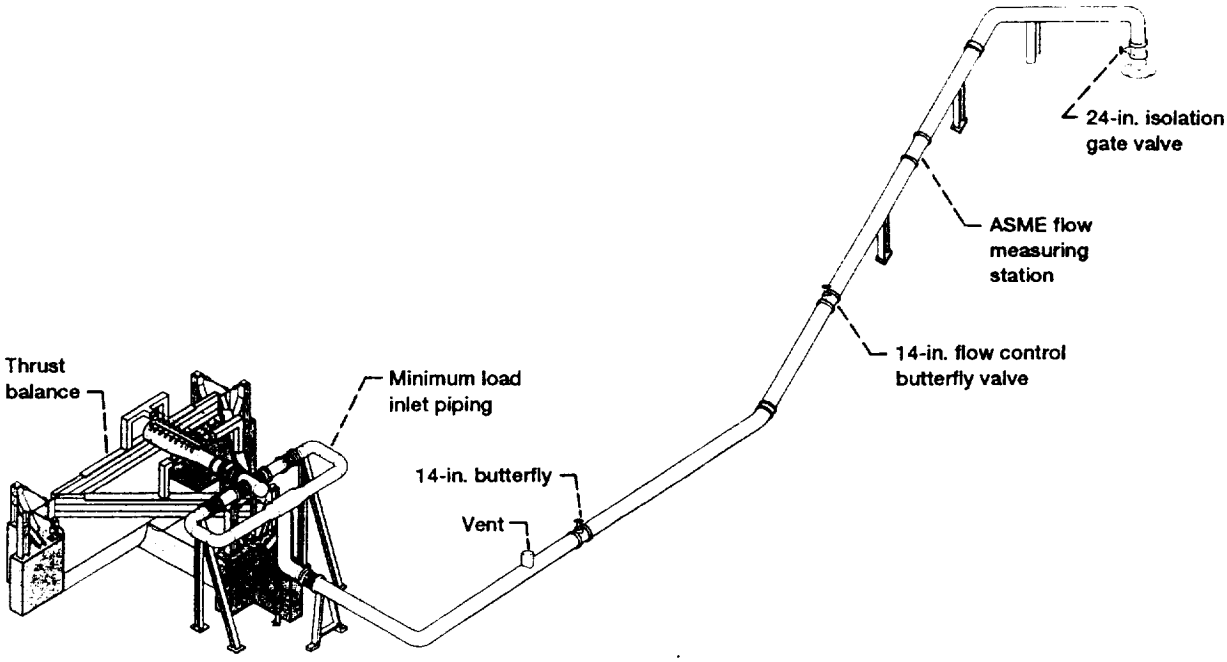

Figure 20.—Air supply system of Powered Lift Facility.

REPORT DOCUMENTATION PAGE

Form Approved
OMB No. 0704-0188

1. AGENCY USE ONLY (*Leave blank*)	2. REPORT DATE	3. REPORT TYPE AND DATES COVERED
	July 1992	Technical Memorandum

4. TITLE AND SUBTITLE
Experimental Performance of Three Design Factors for Ventral Nozzles for SSTOVL Aircraft

5. FUNDING NUMBERS
WU–505–68–32

6. AUTHOR(S)
Barbara S. Esker and Gail P. Perusek

7. PERFORMING ORGANIZATION NAME(S) AND ADDRESS(ES)
National Aeronautics and Space Administration
Lewis Research Center
Cleveland, Ohio 44135–3191

8. PERFORMING ORGANIZATION REPORT NUMBER
E–7085

9. SPONSORING/MONITORING AGENCY NAMES(S) AND ADDRESS(ES)
National Aeronautics and Space Administration
Washington, D.C. 20546–0001

10. SPONSORING/MONITORING AGENCY REPORT NUMBER
NASA TM–105697
AIAA–92–3789

11. SUPPLEMENTARY NOTES
Prepared for the 28th Joint Propulsion Conference and Exhibit cosponsored by AIAA, SAE, ASME, and ASEE. Responsible person, Barbara S. Esker, (216) 433–8707.

12a. DISTRIBUTION/AVAILABILITY STATEMENT
Unclassified - Unlimited
Subject Category 07

12b. DISTRIBUTION CODE

13. ABSTRACT (*Maximum 200 words*)
An experimental study of three variations of a ventral nozzle system for supersonic short-takeoff and vertical-landing (SSTOVL) aircraft was performed on the NASA Lewis Research Center Powered Lift Facility. These test results include the effects of an annular duct flow into the ventral duct, a blocked tailpipe, and a short ventral duct length. An analytical study was also performed on the short ventral duct configuration using the PARC3D computational dynamics code. Data presented include pressure losses, thrust and flow performance, internal flow visualization, and pressure distributions at the exit plane of the ventral nozzle.

14. SUBJECT TERMS
Nozzles; Short takeoff aircraft; Powered lift aircraft; Exhaust systems

15. NUMBER OF PAGES
16

16. PRICE CODE
A03

17. SECURITY CLASSIFICATION OF REPORT	18. SECURITY CLASSIFICATION OF THIS PAGE	19. SECURITY CLASSIFICATION OF ABSTRACT	20. LIMITATION OF ABSTRACT
Unclassified	Unclassified	Unclassified	